Supporting information

Exploring Cation-Anion Redox Processes in One-Dimensional Linear Chain Vanadium Tetrasulphide Rechargeable Magnesium Ion Cathodes

Sunita Dey,[a] Jeongjae Lee,[a] Sylvia Britto,[a,b] Joshua M. Stratford,[a] Evan N. Keyzer,[a] Matthew T. Dunstan,[a] Giannantonio Cibin,[b] Simon J. Cassidy,[c] Mahmoud Elgaml [c], and Clare P. Grey[*, a]

[a]Department of Chemistry, University of Cambridge, Lensfield Road, Cambridge, CB2 1EW, UK
[b]Diamond Light Source, Harwell Science and Innovation Campus, Didcot, UK
[c]Department of Chemistry, University of Oxford, South Parks Road, Oxford, OX1 3QR, UK
*cpg27@cam.ac.uk

Materials and Methods.

Synthesis. VS_4-reduced graphene oxide (rGO) powder was synthesized following the previous report of Rout et al.[1] The composites have 3 wt% rGO content. The particle sizes are in the range of 100-500 nm.[1] K_3VS_4 was synthesized by grinding together stoichiometric quantities of K_2S, V, and S and heating the mixture in a sealed tube at 650 °C for 20 hrs followed by cooling to 250°C and finally quenching in air.[2,3] Similarly, $LiVS_2$ was prepared by heating a mixture of Li_2S, V, and S at 750 °C for 20 hrs, which is followed by a similar cooling procedure.[4] Another model compound, MgS, was synthesized by heating $MgSO_4$ (≥ 99.5%) powder in the stream of CS_2-aerosolised Ar at 800 °C for 4 hrs. The powder was then cooled down, transferred to the glove box, ground and heated again in the stream of CS_2-aerosolised Ar. S powder was used as-received from Sigma-Aldrich.

We have tried to synthesize $Mg_3V_2S_8$ by solid state route using following methods, however, the XRD showed we were not successful to synthesize the ternary compounds we aimed for.[5–7] The powders of the elements Mg, V and S were ground together inside a glovebox, then sealed in a silica tube with the combined powder kept under liquid nitrogen to prevent sulphur subliming. The sample was heated to 600°C (rate 0.5°C/min) and held for 6 days before cooling to room temperature (rate 1°C/min). We have also tried a reaction of MgS + V + S in a tube furnace with the sample in the hot end at 850°C and cold end at 550°C for 1 week. The powders of these elements were sealed in a silica tube, the tube was placed in a tube furnace with the powder at the centre of the furnace in the heating zone and the empty end of the tube away from the centre. The sample was heated at 1°C/min until the hot end reached 600°C, held for 12 hrs then heated at 1°C/min to 850°C and held for 6 days. The method was repeated by decreasing the annealing temperature (440°C followed by 650°C) with faster cooling rate.

Electrode preparation. VS_4 was mixed homogenously with Ketjen Black and PVDF (weight ratio of 80:10:10) using N-Methyl-2-pyrrolidone (NMP, anhydrous, Sigma-Aldrich) and cast on copper foil in a film 150 µm thick. The film was dried at 60ºC under vacuum before VS_4 cathodes were punched out (diameter 1.27 cm and loading of ~ 3 mg/cm^2). Mg ribbon (Sigma Aldrich) was polished by blade to remove the MgO layer and cut into pieces of ˜8 mm X 3 mm X 0.2 mm to fit in 2032 type cells. A 0.25 (M) tetrahydrofuran (THF) solution of magnesium organohalo-aluminate salt, $Mg(AlCl_2EtBu)_2$/THF was used as the electrolyte (the THF is supplied by Sigma Aldrich, ≥ 99.0%, re-distilled in the lab and stored over molecular sieves, and shows a final H_2O content of ˜12 ppm by Karl Fisher titration before making

the electrolyte). Standard stainless steel 2032 coin cells (Cambridge Energy Solutions) were assembled inside the Ar glovebox with borosilicate glass fibre separator (Whatman) soaked on 150 µl electrolyte, 0.5 mm thick spacer, conical spring, plastic gasket and Mg metal as counter electrode. All electrochemical measurements were conducted at ambient temperature using a Lanhe battery cycler (Wuhan Land Electronics Co. Ltd.). Prior to ex situ measurements batteries were disassembled inside the Ar glove box, cycled films were rinsed three times with THF and dried in the glove box pre-chamber (under vacuum) for 30 mins.

X-ray Diffraction (XRD): XRD was carried out using a PANalytical Empyrean powder diffractometer operated at 40 kV and 40 mA with CuKα radiation (wavelength λ=0.154 nm).

X-ray Photoelectron Spectroscopy (XPS). XPS was carried out at Harwell Campus, UK. A Thermo Scientific K-Alpha XPS system with monochromated micro-focused Al-Kα X-ray (1468.7 eV) was used at 72W (12 kV x 6 mA). The instrument was equipped with a 180°, double focusing, and hemispherical analyzer with a 128-channel detector. Fixed Analyzer Transmission mode with pass energy of 40 eV was used. Samples were adhered to a conductive carbon film taped onto an airtight transfer chamber (designed by Thermo Fisher Scientific, total loading area 60 X 60 mm) equipped with X-ray-transparent windows, and were brought down to a measurement pressure of 10^{-8} mbar. The instrument is equipped with a Monatomic and Gas Cluster Ion Source (MAGCIS). Before recording the spectra, cluster cleaning was carried out for 1 min in order to remove any surface contamination. The cleaning uses energy of 4 keV (nearly equivalent to a cluster of 4,000 Ar atoms carrying energy of 1eV/atom). The spot size of measurement was 400 μm^2. Along with a high resolution survey scan, energy specific spectra of S2p and Mg2p were recorded by dedicated scanning (step size 0.1 eV/min) over the energy ranges of 155-168 eV and 46-55 eV respectively. Data processing including background correction (using a Shirley function) and peak fitting (using Gaussian-Lorentzian functions) was performed with the CasaXPS software (version 2.3.15). Surface charging shifts the true binding energy of electrons; a C 1s photoelectron peak position of 284.8 eV is used as an internal reference.

Nuclear Magnetic Resonance (NMR). All the experiments were performed with a BrukerAvance 500 MHz (11.7 T) spectrometer operating at a ^{51}V Larmor frequency of 131.7 MHz at room temperature. Samples were packed into a ZrO_2 rotor inside the Ar-filled glove box. Bruker probes of 1.3 mm and 2.5 mm were used for magic angle spinning (MAS) at 25 kHz and 50 kHz respectively. An echo sequence with a π/2 pulse length of 1.5 µs and recycle delay of 5 s was used. All the spectra were referenced using solid NH_4VO_3 (Sigma-Aldrich, > 99%) resonating at −565.5 ppm as a secondary reference.[8] The carrier frequency was fixed to 163 ppm and 5600 ppm for recording VS_4 and V spectra respectively. Bruker Topspin (version 4.0.7) was used for raw data processing.

Magic angle turning and phase adjusted sideband separation (MATPASS) NMR experiments were also performed at 11.7 T and were rotor-synchronized at a MAS rate of 50 kHz. A series of five π/2 pulses with a pulse length of 1.5 µs was employed. A total of eight t_1 increments were recorded in each experiment with a recycle delay of 0.5 s.

X-ray Absorption Spectroscopy (XAS). Ex situ XAS was carried out at beamline B18 (bending magnet) at Diamond Light Source (DLS), UK. V K and S K edge spectra were measured at ambient temperature in transmission mode and total electron yield (TEY) mode respectively. The energy scans were carried out above and below the absorption edges of V (~5465eV) and S (~2472 eV)

over the span of 950 eV (step size 0.22 eV) and 400 eV (step size 0.15 eV) respectively. For V K edge transmission mode measurements, around 5 mg of active material was scraped off the film, ground homogenously with dried cellulose (approx. 25-30 mg), pressed into 8 mm-diameter pellets (thickness of ~ 1 mm) and, finally, transferred into a custom-built (DLS) transfer chamber with X-ray-transparent windows inside Ar glove box. For S TEY measurements, cathode films were directly adhered to the transfer chamber with conductive tape. The measurement chamber was purged with He in order to minimise background absorption of the incident X-rays. The samples were measured at overpressure of He to avoid air exposure. Beam size was 200 μm X 250 μm. Three consecutive spectra were collected from each sample to improve the signal-to-noise ratio and ensure no beam damage or sample instability. Ionization chamber detectors were used for transmission mode measurements. Simultaneous measurement of a standard V foil and S powder was performed for energy calibration during the XAS recordings. XAS of all the model compounds was recorded under similar conditions. Background correction, energy calibration, data merging, analysis and peak fitting were performed within the Athena program in the Demeter package running IFEFFI.[9]

Pair Distribution Function Analysis (PDF). PDF measurements were performed at beamline I15 at Diamond Light Source, UK at X-ray transmission mode. Samples were packed in a borosilicate capillary (diameter~ 1.0 mm) and sealed with adhesive. Background measurements were taken in an identical empty capillary. Typical exposure time was 100 sec per scan. Measurements were performed with an X-ray beam of 76 keV (λ=0.1631 Å). An amorphous silicon area detector (PerkinElmer) was used to record total scattering data up to a large momentum transfer value (Q_{max} is 41.2 $Å^{-1}$). The data were converted to intensity vs Q. All standard corrections including background, Compton scattering and detector effects were applied. This was followed by Fourier transformation to obtain the G(r). The data were integrated with the Data Analysis Workbench (DAWN)[10] programme and extracted with GudrunX. Structural refinements were performed in PDFGUI[11] and plotted with Vesta 3.[12]

The PDF refinement parameter delta, which corrects for the temperature effect on the correlated motion is kept between 0.2-0.3. An obtained R_w value was implemented as a measure of goodness of fit. R_w values greater than 15 % are usual in PDF results, even in highly crystalline materials. PDF refinements produce much higher R_w values than typical XRD Rietveld refinement as the two methods use different functions to fit the patterns.[13,14]

Computation. Potential stable phases corresponding to the composition $Mg_3V_2S_8$ (i.e. a full reduction of sulphur to S^{2-}) were searched using the evolutionary method as implemented in the USPEX (Universal Structure Predictor: Evolutionary Xtallography) code.[15–17] Ionic relaxations of the generated structures were performed within the framework of Density Functional Theory (DFT) utilizing the Perdew-Burke-Ernzerhof (PBE) functional as implemented in the Vienna Ab initio Simulation Package (VASP) code.[18,19] Projector-augmented wave pseudopotentials with the following valence electrons were used: 2s (Mg), 3s (V), and 2p (S). A plane-wave energy cut-off of 340 eV and *k*-point resolution of <0.05 $Å^{-1}$ was used for the final energy calculation. The starting generation consisted of 50 structures consisting of up to 5 formula units (52 atoms) in all possible space groups except the P1. A total of 64 generations were produced with 50 structures in each generation; the minimisation was deemed complete when a structure was the lowest enthalpy structure for 30 generations. The proportions of evolutionary operators were adjusted automatically as implemented in the USPEX code. Potentials for the electrochemical (insertion and) conversion reactions were calculated within the same theoretical

framework while fully relaxing the structures. Formation energy calculations were also performed under the same theoretical framework.

The phonon calculation on the $Mg_3V_2S_8$ structure was performed using a phonopycode[20] employing the finite-displacement method. A 52-atom supercell was used with a 2×2×2 Monkhorst-Pack grid and an increased plane-wave energy cut-off of 550 eV.

Section 1. Supporting electrochemistry figures

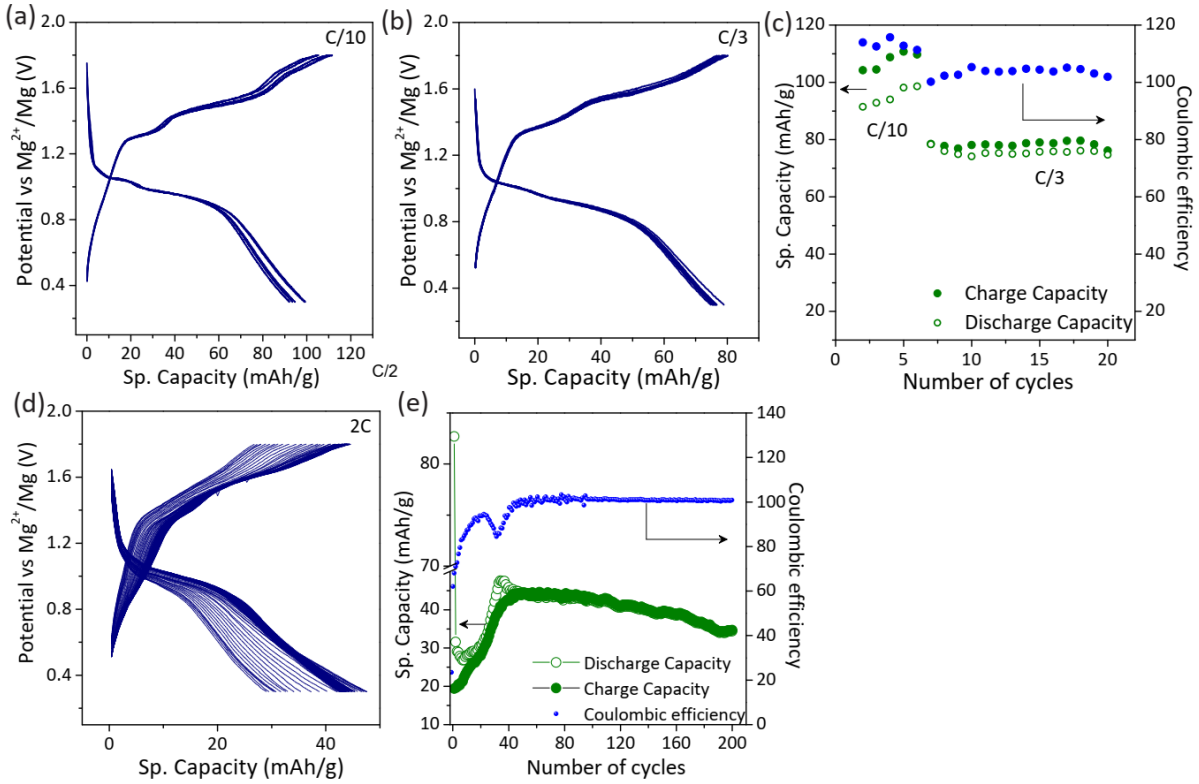

Figure S1. VS_4 galvanostatically cycled at rate of (a) C/10, (b) C/3 and (d) 2C. The variation of charge-discharge specific capacity and Coulombic efficiency with cycle numbers are shown in figures c and e.

Section 2. XANES supporting figures

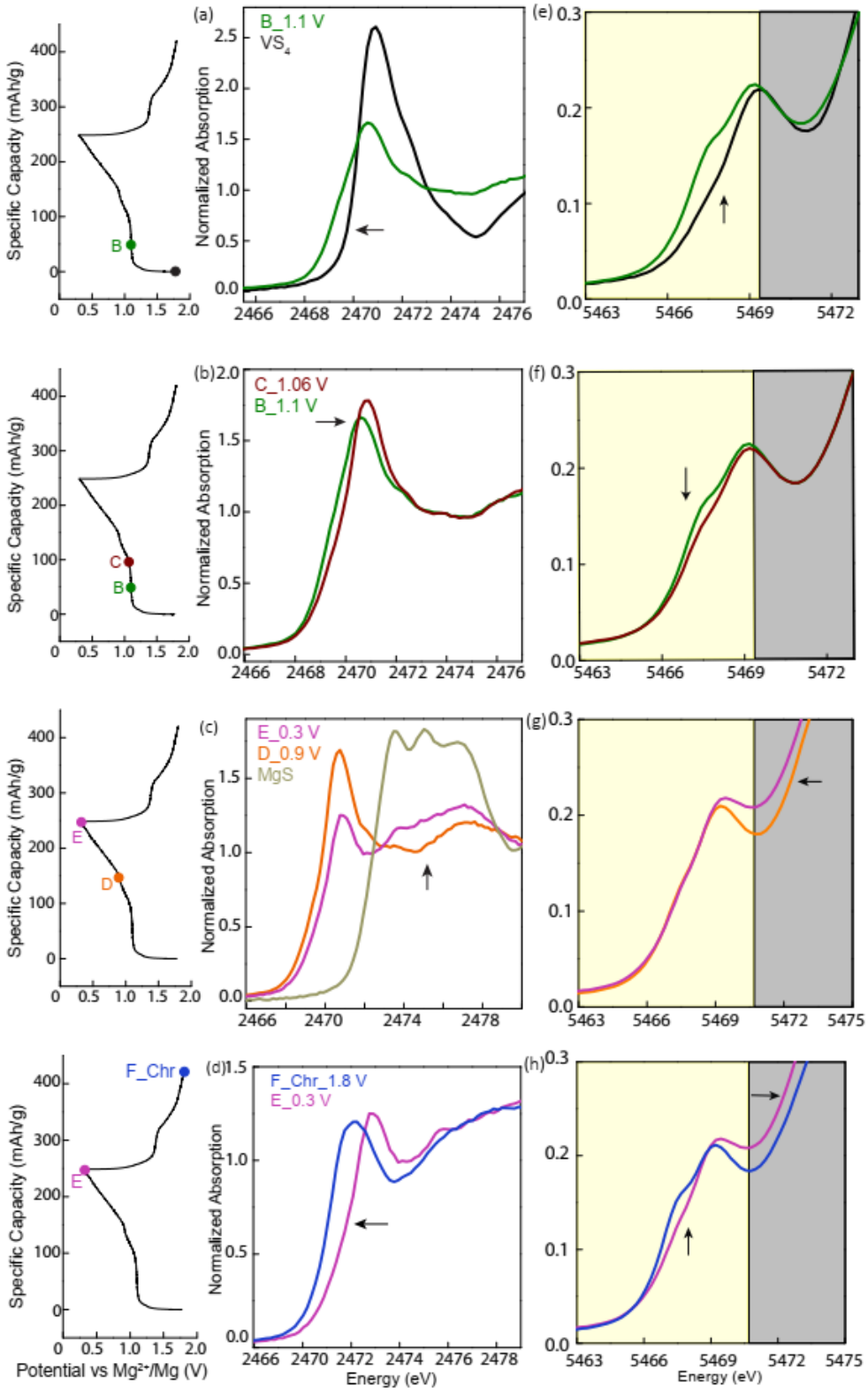

Figure S2. (a-d) S and (e-h) V K edge XANES spectra of VS_4 at various states of charge-discharge. Sudden changes in absorption positions and intensities are marked by arrows.

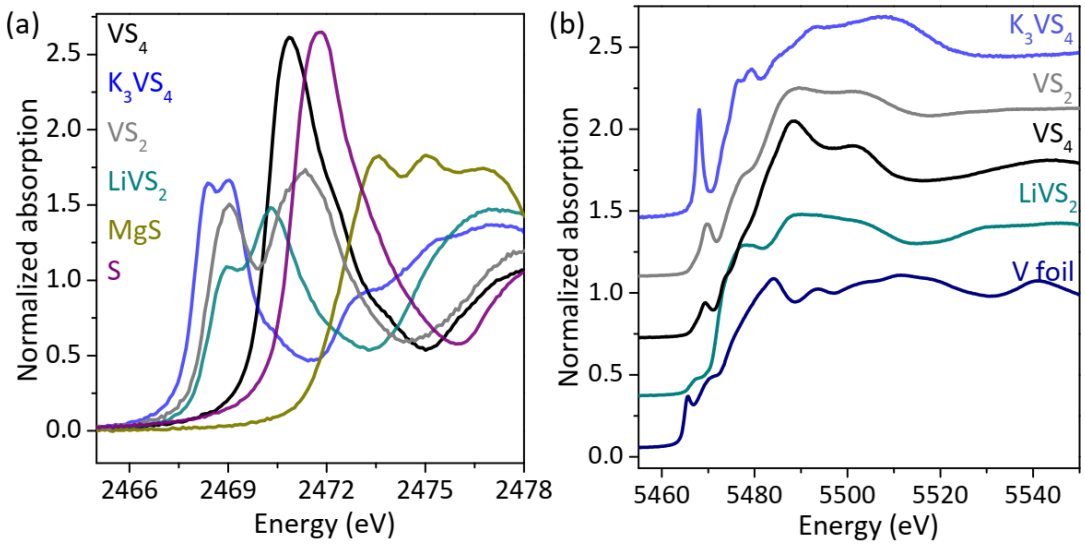

Figure S3. (a) Normalized S K edge and (b) V K edge XANES spectra of model compounds: $LiVS_2$ (V^{3+}, S^{2-}), VS_2 (V^{4+}, S^{2-}), K_3VS_4 (V^{5+}, S^{2-}), VS_4 (V^{4+}, S^{1-}), MgS (S^{2-}), S(0) and V(0).

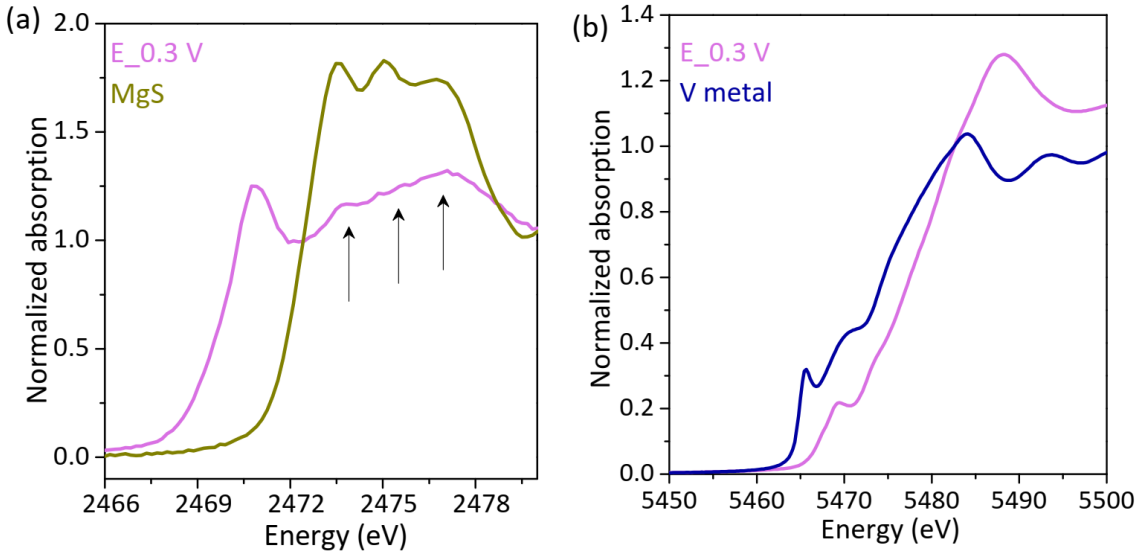

Figure S4. (a) Normalized S K edge XANES spectra of sample E (0.3 V discharged sample) is presented and compared to the model compound MgS. The high energy region of sample E has three distinct energy features due to constructive resonances (marked by arrows), which closely match the absorption features of MgS. (b) Normalized V K edge XANES spectra of sample E in comparison to commercially available body-centred cubic V metal.

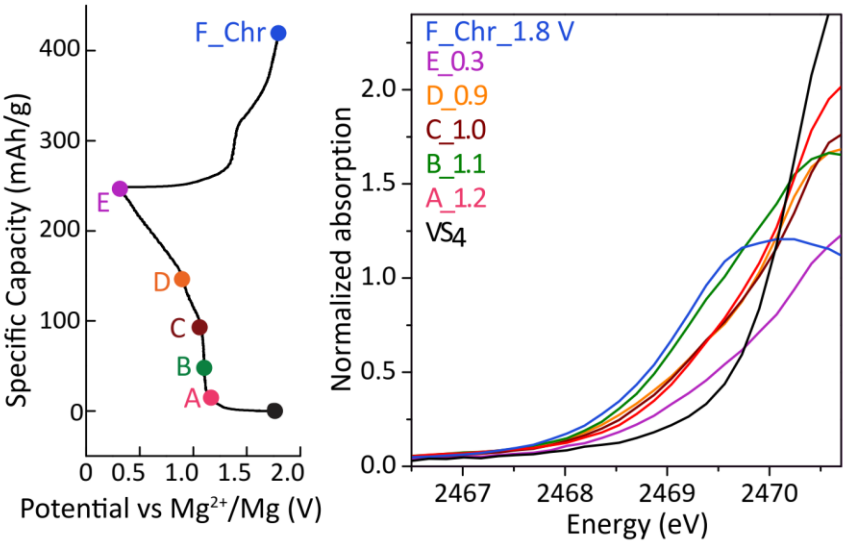

Figure S5. S K edge XANES spectra of VS_4 at different states of charge-discharge to show the absorption in the edge rise energy ranges between 2467-2471 eV.

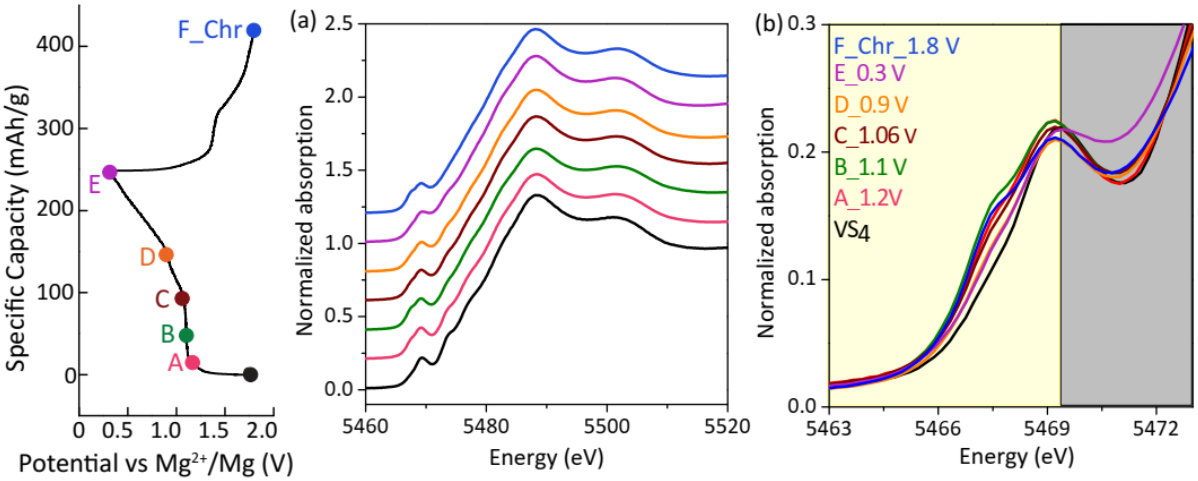

Figure S6. (a) V K edge XAS (5460-5520 eV) spectra of VS_4 at different states of charge-discharge (spectra are vertically offset by 0.2) and (b) V K edge XANES spectra of VS_4 at different states of charge-discharge.

Table S1: Peak area of V^{5+} and V^{4+} in V pre edge XANES spectra and their ratios. The peaks are fitted using a Gaussian function. The area is calculated after background subtraction.

Sample	V^{4+} Peak Area	V^{5+} Peak Area	Decrease in V^{5+} peak area w.r.t VS_4	% Area change of V^{5+} w.r.t. B_1.1 V
VS_4	76.1	15.4*	0	---
A_1.2 V	67.6	32.4	17	-29.6%
B_1.1 V	60.6	39.4	24	0
C_1.06 V	67.7	32.3	16.9	30%
D_0.9 V	70.7	29.3	14	41.6%
E_0.3 V	79	21 **	---	---
F_Chr_1.8 V	60	40	---	

(*) In VS_4, the area for V^{5+} area appears due to crystal field splitting rather than V oxidation.
(**) Sample E has a contribution from V(fcc), introducing an error into this measurement.

Section 3. ^{51}V NMR Supporting figures

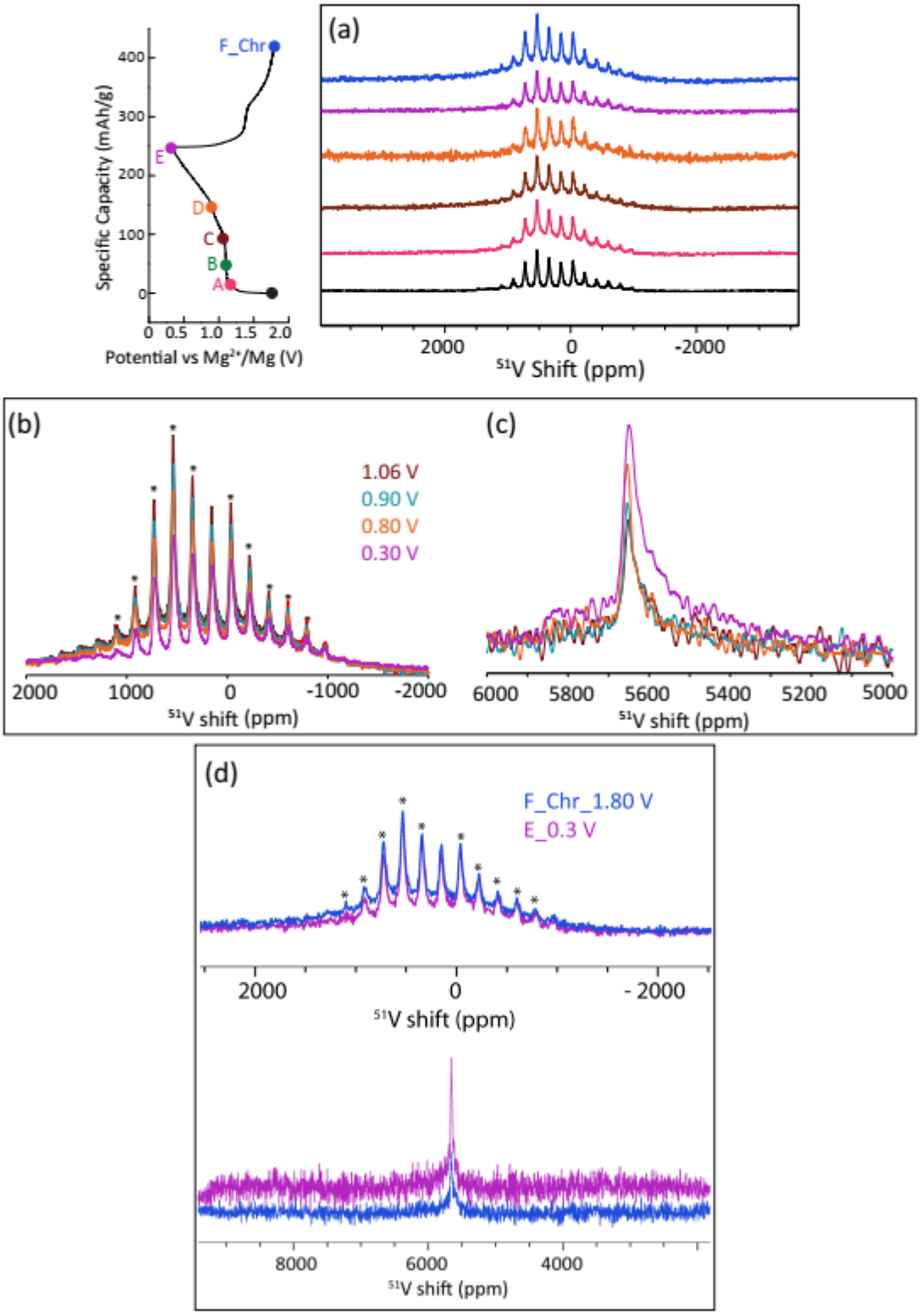

Figure S7. ^{51}V NMR spectra of (a) VS_4 recorded during first charge-discharge cycle at lower Magic angle spinning (MAS) speed of 25 KHz acquired at 11.7 T magnet. Asterisk denotes the side bands. No extra peak appears on cycling at this MAS, aside from the peaks inherent to VS_4. ^{51}V NMR intensity of (b) VS_4

decreases and (c) V(fcc) metal increases gradually during first discharge processes. (d) ^{51}V NMR intensity of VS_4 remains similar (top) and V(fcc) metal decreases (bottom) on moving from the end of discharging (E_0.3 V) to charging (F_1.8 V). All the spectra are normalized w.r.t. number of scans and weight of the sample.

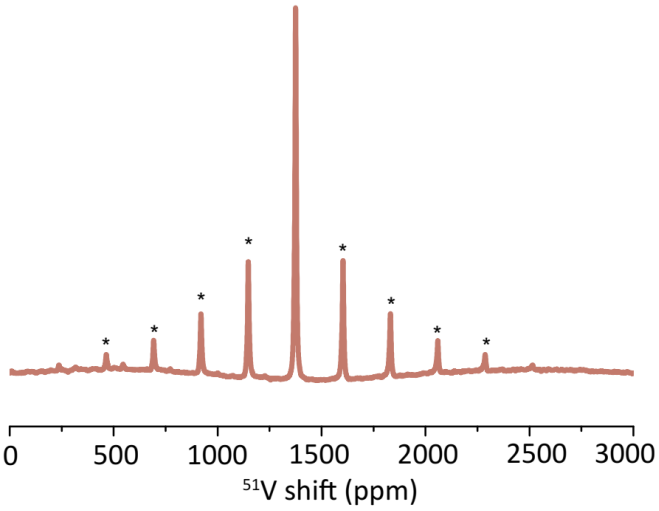

Figure S8. ^{51}V NMR of K_3VS_4 (model compound) measured at 9.4 T field strength. Asterisks denote the side bands.

Table S2. The predicted composition of the products formed during various state of discharge in the Mg/VS_4 system and percentage of unreacted VS_4. The total Mg content in the products is calculated assuming the unreacted VS_4 and the number of Mg ions that have been inserted determined from the electrochemistry. The average oxidation state of the different elements is given for the intermediate phase (see text for assumptions and relevant calculations).

Sample	Total Mg content in the products (From Electrochemistry)	Composition of the product(s)	Unreacted VS_4
B_1.1 V	0.44	$Mg_{0.44}^{2+}V^{5+}S_4^{1.5-}$	~ 62 %
C_1.06 V	0.86	$Mg_{0.86}^{2+}V^{4.58+}S_4^{1.5-}$	~ 62 %
E_0.3 V	1.56	$Mg_{0.86}^{2+}V^{4.58+}S_4^{1.5-}$ + 0.15(V+4MgS)	~ 47 %

The compositions shown in Table S2 are proposed based on the following details acquired from multiple characterization techniques. The calculations of the residual VS_4 content were performed as follows. At point C and point E, the VS_4 concentration has decreased by 38% and 60%, as calculated based on the intensity of the isotropic ^{51}V NMR VS_4 resonance (163 ppm). We also performed a linear combination fitting (LCF) of the S XANES data, in order to calculate the remaining percentage of VS_4 at points B and C. The LCF was performed by taking the pristine VS_4 and 1.8 V charged sample (point F) as the standards where the pristine and 1.8 V charged sample (point F) contain 100% and 40% of VS_4, respectively (point F contains 40% VS_4, same as present in point E and quantified by NMR). LCF shows ~ 35-40% of VS_4 has being reacted at point B and C, which is in line with the NMR results. The relative

change in the % of VS_4 at various SOCs can also be evaluated by examining the S XANES spectra (Figure S2) which show a nearly ~40 % drop in the normalized absorption intensity at points B and C, which further drops to ~ 55% at point E.

The electrochemistry data shows that 0.17 mol Mg/mol VS_4 are inserted on discharging to 1.1 V (point B, Figure 2a) and XANES (NMR) indicates ~ 38 % of VS_4 has being reacted at this point. Assuming that all the V in the $Mg_{0.44}VS_4$ intermediate is present in a +5 oxidation state (supported by V XANES and V NMR), from charge balancing this gives a composition of intermediate at point B of $\mathrm{Mg}_{0.44}^{2+}\mathrm{V}^{5+}\mathrm{S}_4^{1.5-}$. Sample B showed a broad S^{2-x} XPS peak with a binding energy intermediate between that expected for $[S_2]^{2-}$ and S^{2-} peaks, a S XANES absorption at ~2469.2 eV (higher in energy than the S^{2-} peak of K_3VS_4 observed at 2468.7 eV, Figure S3a) and the most intense V-S PDF correlation at 2.28 Å, which is intermediate between the V-S bond length observed for K_3VS_4 (~ 2.17 Å) and VS_4 (~ 2.40 Å).

Moving from point B to C, the electrochemistry shows that an extra 0.16 mol Mg has been added/mol VS_4. No extra VS_4 is reduced from point B to C, hence, all the current must have been utilized to reduce $\mathrm{Mg}_{0.44}^{2+}\mathrm{V}^{5+}\mathrm{S}_4^{1.5-}$ (composition at point B). The V^{5+} NMR signal has largely disappeared at point C, suggesting that the vanadium centers are reduced giving a composition of $\mathrm{Mg}_{0.86}^{2+}\mathrm{V}^{4.58+}\mathrm{S}_4^{1.5-}$ (V reduction). The V^{5+} pre edge peak area has been decreased by ~ 30 % and ~ 42% by moving from point B to C and from point B to D respectively (Table S1), corroborating the vanadium reduction of the proposed intermediate.

Moving from point C to E, the electrochemistry shows that an extra 0.50 mol Mg (i.e. 0.83-0.33= 0.50) has been intercalated/mol VS_4. As a further complication, during the 1.05 V voltage plateau, V+MgS conversion occurs alongside the reaction to form, or further reduction of, the intermediate phase. The V metal concentration seen by ^{51}V NMR is smaller for C, again confirming that most of the electrons are consumed via reduction of the intermediate, but is noticeably larger at composition E (Figure S7). 53 % of VS_4 has been magnesiated (in total) up to point E, and around 15 % (i.e. 53 -38 = 15%) has reacted from point C to E. We first assume that all of extra VS_4 consumption involves reaction to V(fcc)+MgS; however, this reaction requires approximately 0.60 mol of Mg should have been reacted while moving from point C to E, while only 0.50 mol was measured via the electrochemistry. This small error (given all of the errors in the estimations) is consistent with the presence of some vanadium metal already at point C, and some further reaction of the intermediate (which consumes less Mg), i.e., in practice two simultaneous reactions are going on as discussed above. Since there are many competing reactions, the composition of the intermediate phase given in Table S2 simply assumes that the reaction from C to E involves V formation only. If we instead assume that the V concentration is still negligible at point E, then on the basis of the total number of electrons (and thus Mg ions) that have reacted with 53% of the VS_4 (0.83 Mg per f.u. of VS_4, and thus 1.56 Mg per f.u. of VS_4), the composition of the intermediate corresponds to $Mg_{1.57}VS_4$. The value in Table S2 and this value likely represent the compositional bounds at this point. Ultimately, there are too many variables to allow the stoichiometry to pinned down with more confidence, but the above analysis demonstrates that compositions close to $Mg_3V_2S_8$ are feasible with the magnesiation levels achieved in this study.

Section 4. Supporting figures of XPDF and structural calculations

Table S3. Structural parameters of pristine VS_4 obtained from PDF refinement (R_w = 34.1%) in comparison with literature report (ICSD 16797).

Lattice parameters	Literature Structure	PDF refinement
a/Å	6.780	6.75 (1)
b/Å	10.42	10.40(1)
c/Å	12.11	12.08(2)
β/°	100.8	100.7(1)

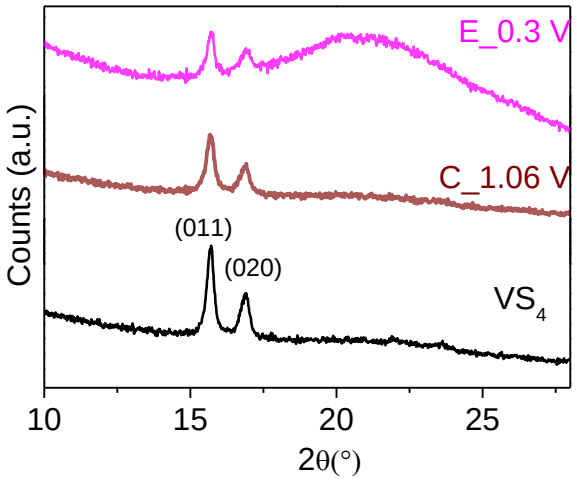

Figure S9. X-ray diffraction pattern of VS_4 taken during first electrochemical discharge at intermediate voltage (point C_1.06V) and end of discharge (Point E_0.3 V).

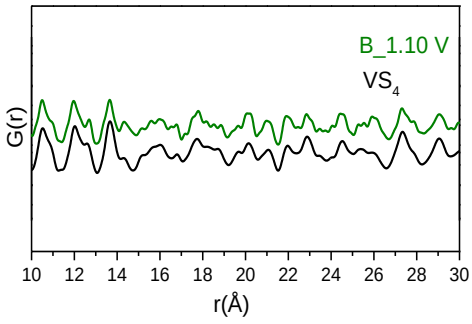

Figure S10. High r (7-50 Å) PDF correlations of 1.1 V discharged VS_4 and uncycled sample prepared under same conditions as of cycled samples.

Table S4. Proposed reaction pathways for the formation of various ternary Mg-V-S compositions as a product of the reactions between VS_4 and Mg. Ternary Mg-V-S compositions are selected from materials project databases.[21] These reaction pathways are simulated and calculated voltages are

close to the VS_4 discharge plateau. The oxidation state of S is -2 and V is either +4 or lower in the Mg-V-S compositions.

Ternary Mg-V-S materials	E above hull (eV)	Proposed reaction	Voltage (V)
$Mg(VS_2)_4$	0.057	$9Mg + 4VS_4 \rightarrow Mg(VS_2)_4 + 8MgS$	1.33
$Mg(VS_2)_2$	0.117	$5Mg + 2VS_4 \rightarrow Mg(VS_2)_2 + 4MgS$	1.28
$MgVS_3$	0.222	$2Mg + VS_4 \rightarrow MgVS_3 + MgS$	1.11
MgV_2S_5	0.261	$4Mg + 2VS_4 \rightarrow MgV_2S_5 + 3MgS$	1.13

Table S5. Unit cell details of USPEX-generated $Mg_3V_2S_8$ structure.
Space group H-M "C 1 c 1"; Cell lengths are a = 7.604(5) Å, b = 13.3501(6) Å, c = 12.3812(1); Cell angles are α=γ= 90.0°, β=106.68(8) °; Unit cell volume is 1204.012(9) $Å^3$

Label	Symbol	Multiplicity	x	y	z
Mg1	Mg	4	0.08233	0.21462	0.23908
Mg2	Mg	4	0.33120	0.46327	0.23354
Mg3	Mg	4	0.85245	0.46201	0.28750
V1	V	4	0.20328	0.37418	0.43921
V2	V	4	0.74557	0.45431	0.05282
S1	S	4	0.78121	0.39932	0.62034
S2	S	4	0.51405	0.11872	0.61756
S3	S	4	0.06706	0.11931	0.63075
S4	S	4	0.88315	0.19988	0.85682
S5	S	4	0.44132	0.20198	0.88688
S6	S	4	0.16916	0.47264	0.88203
S7	S	4	0.63154	0.44862	0.86479
S8	S	4	0.29364	0.37267	0.62282

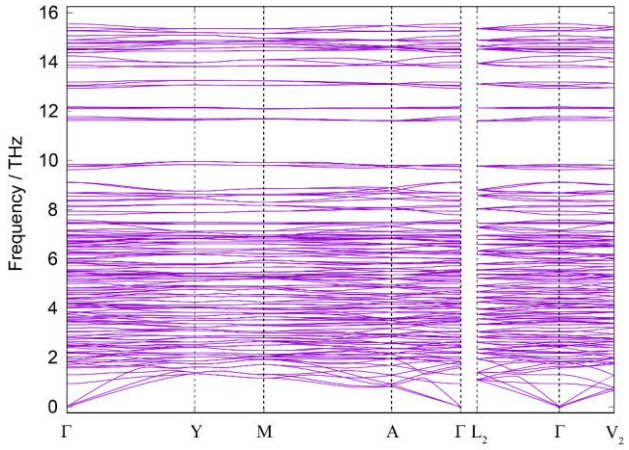

Figure S11. Calculated phonon dispersion curve of the newly found $Mg_3V_2S_8$ phase.

Table S6. The details of the lattice parameters resulting from PDF refinements of $Mg_3V_2S_8$ intermediates generated due to discharging and charging of VS_4 at various potentials. The unit cell of $Mg_3V_2S_8$ for samples B, E and F as obtained after subtracting the contribution of V metal from total PDF data. The lattice parameters of theoretically calculated $Mg_3V_2S_8$ structure are also given for comparison.

Lattice parameters	VS_4	$Mg_3V_2S_8$ (calculated)	1.1 V discharged (Sample B)	0.3 V discharged (Sample E)	1.8 V charged (Sample F)
a/Å	6.75	7.60	7.22(0.1)	7.43 (0.03)	7.42(0.14)
b/Å	10.40	13.35	13.65(0.19)	13.68(0.05)	13.76(0.2)
c/Å	12.08	12.38	12.07(0.2)	11.97(0.05)	12.08(0.2)
β/°	100.7	106.68°	104.45(1.2)	106.3 (0.4)	106.938(1.5)
Unit cell volume/ $Å^3$	848.01	1204.01	1150.97	1165.01	1181.788

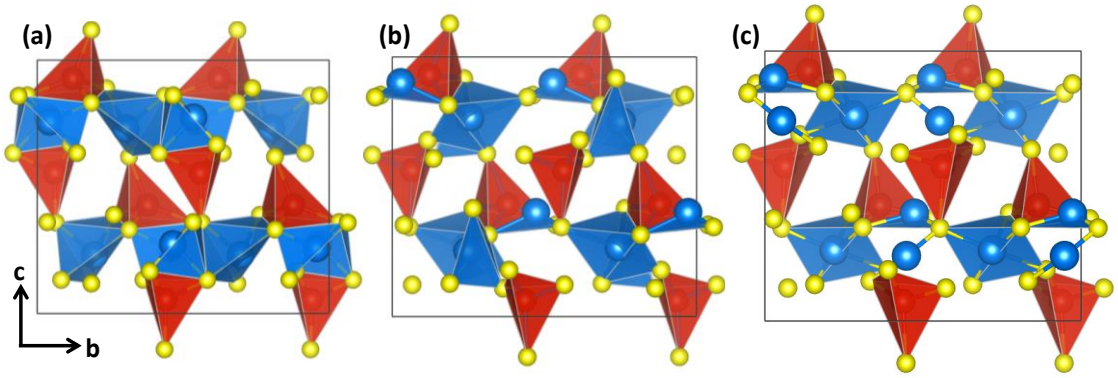

Figure S12. (a-c) The unit cell of $Mg_3V_2S_8$ for samples B, E and F as obtained after subtracting the contribution of V metal from total PDF data. Mg, V and S atoms are represented by blue, red and yellow balls respectively.

Table S7. Details of the structure parameters resulting from refinement of XPDF data of 1.1 V discharged VS_4 (sample B). The XPDF pattern is simulated with the calculated $Mg_3V_2S_8$ unit cell parameters considering triclinic space group. Refined lattice parameters are a = 7.22(0.1) Å, b = 13.65(0.1) Å, c = 12.07(0.2) Å and β = 104.45(1.2)°. The corresponding atomic coordinates and thermal parameters are shown in the table.

element	x	y	z	$U_{11}/U_{22}/U_{33}$
Mg	0.157029	0.202173 (0.053)	0.232133	0.01
Mg	0.359147	0.462753 (0.045)	0.253571	0.01
Mg	0.87648	0.463017 (0.034)	0.274256	0.01
V	0.252399	0.376632 (0.015)	0.434263	0.01
V	0.696435	0.440671 (0.024)	0.0553856	0.01
S	0.827575	0.419093 (0.035)	0.635695	0.01
S	0.464334	0.116232 (0.024)	0.666925	0.01

S	0.0133798	0.136265 (0.036)	0.636505	0.01
S	0.95139	0.186582 (0.033)	0.825146	0.01
S	0.443363	0.232354 (0.044)	0.886891	0.01
S	0.234768	0.468975 (0.038)	0.861305	0.01
S	0.59474	0.435394 (0.034)	0.85671	0.01
S	0.3298	0.309813 (0.034)	0.621227	0.01

Table S8. Details of the structure parameters resulting from refinement of XPDF data of 0.3 V discharged VS_4 (sample E). The XPDF pattern is modelled by 2 phases. One phase is V (fcc) structure of a = 3.616 (1) Å (space group Fm-3m). Another phase is modelled with the $Mg_3V_2S_8$ unit cell parameters considering triclinic space group. Refined lattice parameters are a = 7.43(0.03) Å, b = 13.68(0.05) Å, c = 11.97(0.05) Å and β = 106.3(0.4)°. The corresponding atomic coordinates and thermal parameters are shown in the table.

element	x	y	z	$U_{11}/U_{22}/U_{33}$
Mg	0.144183	0.24427 (0.012)	0.266189	0.01
Mg	0.44091	0.472462 (0.013)	0.402202	0.01
Mg	0.659172	0.249069 (0.012)	0.255014	0.01
V	0.205841	0.377034 (0.0087)	0.432474	0.01
V	0.712708	0.435247 (0.0064)	0.0621925	0.01
S	0.813701	0.435119 (0.0065)	0.623259	0.007
S	0.520533	0.116117 (0.0078)	0.679577	0.007
S	-0.00536003	0.136402 (0.0076)	0.610155	0.007
S	0.937928	0.184388 (0.0086)	0.812581	0.007
S	0.450358	0.235691 (0.0072)	0.917755	0.007
S	0.235757	0.463083 (0.0097)	0.855806	0.007
S	0.59626	0.444026 (0.0065)	0.845199	0.007
S	0.350418	0.311283 (0.0086)	0.627239	0.007

Table S9. Details of the structure parameters resulting from refinement of XPDF data of 1.8 V charged sample (sample F). The XPDF pattern is modelled by 2 phases. One phase is V (fcc) structure of a = 3.616(1) Å (space group Fm-3m). Another phase is modelled with the $Mg_3V_2S_8$ unit cell parameters considering triclinic space group. Refined lattice parameters are a = 7.42(0.14) Å, b = 13.76(0.2) Å, c = 12.08(0.2) Å and β = 106.938(1.5)°. The corresponding atomic coordinates and thermal parameters are shown in the table.

element	x	y	z	$U_{11}/U_{22}/U_{33}$
Mg	0.156997	0.214298 (0.04)	0.258575	0.01
Mg	0.432619	0.484609 (0.05)	0.397734	0.01
Mg	0.670835	0.447159 (0.029)	0.242321	0.01
V	0.231754	0.361369 (0.016)	0.436496	0.01
V	0.70051	0.438078 (0.016)	0.0682853	0.01
S	0.864298	0.422664 (0.025)	0.62208	0.01
S	0.510869	0.107042 (0.025)	0.687042	0.01

S	-0.0347132	0.172253 (0.025)	0.647554	0.01
S	0.947221	0.197018 (0.025)	0.855617	0.01
S	0.429522	0.228747 (0.026)	0.905071	0.01
S	0.205653	0.473298 (0.025)	0.878822	0.01
S	0.61426	0.444878 (0.032)	0.840586	0.01
S	0.311075	0.345602 (0.022)	0.637294	0.01

Section 4. Additional figures

Table S10. Mg interstitial sites in VS_4, ranked by average similarity to Mg sites in $Mg_3V_2S_8$, calculated using Voronoi-based local structural and chemical similarity metric.

Site	a	b	c	Sim(average)	Sim(max)
1	0.483669674	0.246493308	0.636012508	0.218872165	0.224135085
2	0.05096069	0.9620169	0.499759646	0.215373646	0.220552443
3	0.666662463	0.626086725	0.564581664	0.209819234	0.214864471
4	0.248947817	0.01157974	0.862064339	0.20472833	0.209651152
5	0.982287251	0.04497474	0.145091221	0.203694479	0.208592442
6	0.152224094	0.740882587	0.87140414	0.201020964	0.205854641
7	0.492723273	0.118348492	0.864232822	0.198574991	0.203349852
8	0.034014665	0.506471036	0.803773925	0.197680504	0.202433857
9	0.982287251	0.956832905	0.145091221	0.193498213	0.198151001
10	0.713178133	0.633510067	0.876792224	0.19183039	0.196443073
11	0.893308233	0.613071131	0.858118039	0.187220917	0.191722763
12	0.923603816	0.711943715	0.565309486	0.186532871	0.191018172
13	0.426131726	0.010598404	0.853254934	0.183854644	0.188275546
14	0.891058919	0.944892251	0.394742504	0.182054789	0.186432413
15	0.665318375	0.375808571	0.828155371	0.181250504	0.185608788
16	0.740704794	0.513588252	0.583678092	0.179211921	0.183521185
17	0.737121021	0.229306764	0.807290538	0.178881846	0.183183174
18	0.007819121	0.806958998	0.6700491	0.17868103	0.182977529
19	0.762433556	0.129989982	0.824558537	0.174224267	0.1784136
20	0.00E+00	0.733489795	0.75	0.171582351	0.175708158

Table S11. DFT computed electrochemical potentials for various Mg conversion/insertion reactions involved. For insertion reactions, values for the most stable insertion product for each stoichiometry are shown.

Reaction	DFT potential / V
$VS_4+1.5Mg \rightarrow 0.5Mg_3V_2S_8$	1.10
$VS_4+4Mg \rightarrow V(fcc)+4MgS$	1.04
$VS_4+4Mg \rightarrow V(bcc)+4MgS$	1.08

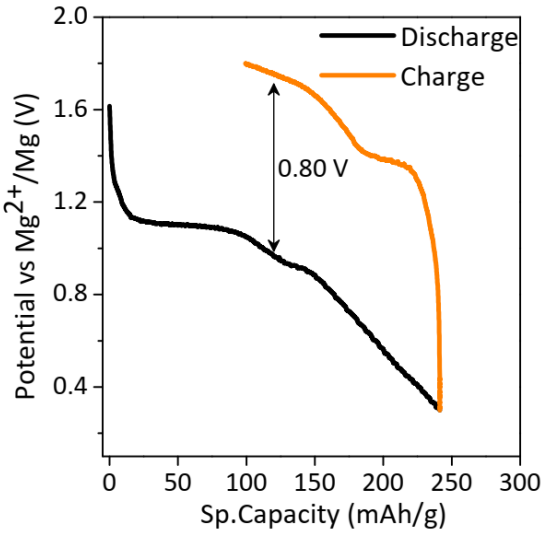

Figure S13. Voltage-capacity curve of VS_4 cathode cycling against Mg anode at 293 K. The curve is for the first cycle. The arrow marks the voltage hysteresis between discharge and charge.

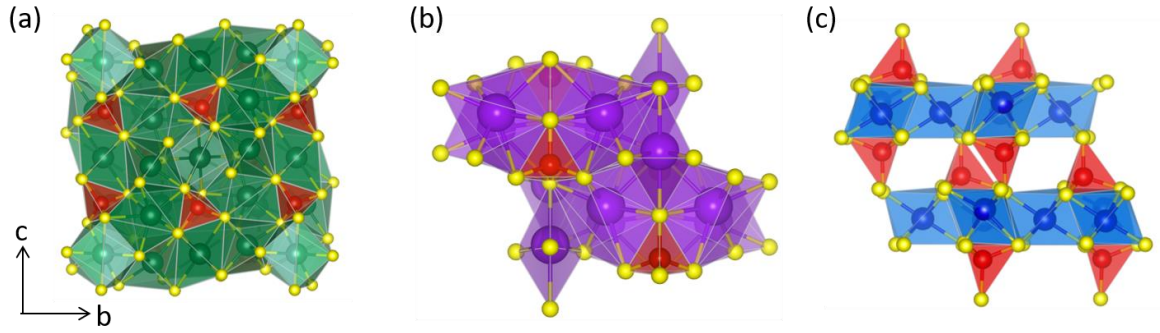

Figure S14. Crystal structure of (a) Na_3VS_4 (space group P-421c, ICSD 84298), (b) K_3VS_4 (space group Pmcn, ICSD 74678) and (c) $Mg_3V_2S_8$. V and S atoms are marked by red and yellow colour respectively. Na, K and Mg atoms are indicated by green, violet and blue colour respectively. Na_3VS_4 crystallizes in tetragonal structure closely packed in all three directions where VS_4 T_d are separated by the NaS_6 Oh. K_3VS_4 crystallizes in a closely packed orthorhombic structure consisting of VS_4 T_d separated by KS_7 and KS_5 units.

Table S12. Vanadium sulphur bond distances for different oxidation states of V and S. The data are obtained from CIF files of known structures. $BaVS_3$ (ICSD 86796), VS_2 (ICSD 68713), K_3VS_4 (ICSD 74678), VS_4 (ICSD 16797).

Materials	V-S bond distances (Å)	V oxidation state	S oxidation state
VS_2	~2.36	+4	-2
$BaVS_3$	~2.37	+4	-2
K_3VS_4	~2.15 (V-S1), ~2.163 (V-S2), ~2.147 (V-S3)	+5	-2
VS_4	~2.40	+4	-1

References.

(1) Rout, C. S.; Kim, B.-H.; Xu, X.; Yang, J.; Jeong, H. Y.; Odkhuu, D.; Park, N.; Cho, J.; Shin, H. S. Synthesis and Characterization of Patronite Form of Vanadium Sulfide on Graphitic Layer. *J. Am. Chem. Soc.* **2013**, *135* (23), 8720–8725.

(2) Van den Berg, J. M.; De Vries, R. The Crystal Structure of K3VS4. *Proc. Kon. Ned. Akad. Wet. B* **1964**, No. B67, 178–180.

(3) Britto, S.; Leskes, M.; Hua, X.; Hébert, C.-A.; Shin, H. S.; Clarke, S.; Borkiewicz, O.; Chapman, K. W.; Seshadri, R.; Cho, J. Multiple Redox Modes in the Reversible Lithiation of High-Capacity, Peierls-Distorted Vanadium Sulfide. *J. Am. Chem. Soc.* **2015**, *137* (26), 8499–8508.

(4) Gupta, A.; Mullins, C. B.; Goodenough, J. B. Electrochemical Probings of Li1+xVS2. *Electrochim. Acta* **2012**, *78*, 430–433.

(5) Herzog, S.; Näther, C.; Dürichen, P.; Bensch, W. Synthesis and Crystal Structure of a New Alkali Metal Tantalum Sulfide: Na3TaS4. *Z. Anorg. Allg. Chem.* **1998**, *624* (12), 2021–2024.

(6) Latroche, M.; Ibers, J. A. Syntheses and Structures of K3MO4 (M= Niobium, Tantalum; Q= Sulfur, Selenium). *Inorg. Chem.* **1990**, *29* (8), 1503–1505.

(7) Omloo, W.; Jellinek, F. Spectra of Some Tetrathiometallates and Tetraselenometallates. *Recl. des Trav. Chim. des Pays-Bas* **1969**, *88* (10), 1205–1212.

(8) Hayashi, S.; Hayamizu, K. 51V NMR Chemical Shift and Anisotropy in Solid Metavanadates. *Bull. Chem. Soc. Jpn.* **1990**, *63* (3), 961–963.

(9) Ravel, B.; Newville, M. ATHENA, ARTEMIS, HEPHAESTUS: Data Analysis for X-Ray Absorption Spectroscopy Using IFEFFIT. *J. Synchrotron Radiat.* **2005**, *12* (4), 537–541.

(10) Basham, M.; Filik, J.; Wharmby, M. T.; Chang, P. C. Y.; El Kassaby, B.; Gerring, M.; Aishima, J.; Levik, K.; Pulford, B. C. A.; Sikharulidze, I. Data Analysis Workbench (DAWN). *J. Synchrotron Radiat.* **2015**, *22* (3), 853–858.

(11) Farrow, C. L.; Juhas, P.; Liu, J. W.; Bryndin, D.; Božin, E. S.; Bloch, J.; Proffen, T.; Billinge, S. J. L. PDFfit2 and PDFgui: Computer Programs for Studying Nanostructure in Crystals. *J. Phys. Condens. Matter* **2007**, *19* (33), 335219.

(12) Momma, K.; Izumi, F. VESTA 3 for Three-Dimensional Visualization of Crystal, Volumetric and Morphology Data. *J. Appl. Crystallogr.* **2011**, *44* (6), 1272–1276.

(13) Allan, P. K.; Griffin, J. M.; Darwiche, A.; Borkiewicz, O. J.; Wiaderek, K. M.; Chapman, K. W.; Morris, A. J.; Chupas, P. J.; Monconduit, L.; Grey, C. P. Tracking Sodium-Antimonide Phase Transformations in Sodium-Ion Anodes: Insights from Operando Pair Distribution Function Analysis and Solid-State NMR Spectroscopy. *J. Am. Chem. Soc.* **2016**, *138* (7), 2352–2365.

(14) Petkov, V.; Gateshki, M.; Choi, J.; Gillan, E. G.; Ren, Y. Structure of Nanocrystalline GaN from X-Ray Diffraction, Rietveld and Atomic Pair Distribution Function Analyses. *J. Mater. Chem.* **2005**, *15* (43), 4654–4659.

(15) Oganov, A. R.; Glass, C. W. Crystal Structure Prediction Using Ab Initio Evolutionary Techniques: Principles and Applications. *J. Chem. Phys.* **2006**, *124* (24), 244704.

(16) Oganov, A. R.; Lyakhov, A. O.; Valle, M. How Evolutionary Crystal Structure Prediction Works—and Why. *Acc. Chem. Res.* **2011**, *44* (3), 227–237.

(17) Lyakhov, A. O.; Oganov, A. R.; Stokes, H. T.; Zhu, Q. New Developments in Evolutionary Structure Prediction Algorithm USPEX. *Comput. Phys. Commun.* **2013**, *184* (4), 1172–1182.

(18) Perdew, J. P.; Burke, K.; Ernzerhof, M. Generalized Gradient Approximation Made Simple. *Phys. Rev. Lett.* **1996**, *77* (18), 3865.

(19) Kresse, G.; Hafner, J. Ab Initio Molecular Dynamics for Liquid Metals. *Phys. Rev. B* **1993**, *47* (1), 558.

(20) Togo, A.; Tanaka, I. First Principles Phonon Calculations in Materials Science. *Scr. Mater.* **2015**, *108*, 1–5.

(21) Jain, A.; Ong, S. P.; Hautier, G.; Chen, W.; Richards, W. D.; Dacek, S.; Cholia, S.; Gunter, D.; Skinner, D.; Ceder, G.; Persson, K. A. Commentary: The Materials Project: A Materials Genome Approach to Accelerating Materials Innovation. *APL Mater.* **2013**, *1* (1), 011002. https://doi.org/10.1063/1.4812323.